修士論文

Design of Photonic Crystal Nanocavities for Highly-Efficient Surface-Emitting Light Sources

（高効率面発光型素子へ向けたフォトニック結晶ナノ共振器の設計）

平成１８年２月３日提出

指導教官　荒川　泰彦　教授

工学系研究科電子工学専攻

４６７６１　タンデーシーヌラット　アニワット

Table of Contents

Chapter 1

Introduction

1.1 Background of This Research

Since the pioneering work of Purcell [1] describing the modification of the coupling between the electromagnetic field and an emitter placed inside a cavity and the discovery of photonic band gap material [2], the use of photonic band gap structure as a cavity to control spontaneous emission has become an active field of research. The photonic band gap structure or called "Photonic crystal" is a periodic arrangement of dielectric media in wavelength-scale that can affect the propagation of electromagnetic waves in the same way as electron experiencing a periodic potential in a semiconductor crystal. In analogy with allowed and forbidden energy bands in electronic system, photonic crystal can provide a range of wavelengths, in which no light modes are allowed to propagate through the structures. This range in frequencies is called photonic band gap. By introducing a defect to the structure, a perfectly periodic lattice can be destroyed and a cavity is formed. A defect may permit localized modes with frequencies inside photonic band gap to exist. In past ten years, with the maturation of nanometer-size photonic crystal fabrication, there has been strong interest in creating optical nanocavities for spontaneous emission manipulation. Nanocavities that can create very high quality factor (Q-factor) with wavelength-size mode volume, in other words, a large Purcell factor, are expected to be promising structures for nanophotonic devices, such as low-threshold lasers [3], [4], single photon sources [5], [6], and etc., because nanocavities can help reducing threshold of lasers, increasing repetition rate of single photon emitters, and improving their efficiency. Photonic crystal slab defect cavities have a great potential to achieve that goal due to their simplicity in fabrication and their ability to achieve strong confinement of light in three dimensions. Several groups have already reported the design of ultra high Q-factor photonic crystal slab nanocavities together with mode volume of the order of the cubic wavelength [7]-[13]. However, the efficiency of those devices has been a long-standing problem. Such structures are well known to have low efficiency due to low extraction efficiency and complicated radiation pattern. Moreover, all those cavities need a modification of the defect structure to achieve

such high Q-factor. Nonetheless, owing to the sensitivity of the high-Q modes to the surrounding structural parameters, these designs require a precise control of position and size of air holes in practical fabrication, in which the Q-factor and the efficiency are significantly degraded when the structural parameters are deviated from their ideal setups. In other words, these structures lack of robustness in practical systems. In addition, radiation pattern of output light is another key obstacle to achieve highly-efficient light sources, because it determines the collection efficiency. In order to efficiently collect the output light radiated out from the cavity, a simple radiation pattern, which has Gaussian-like distribution, is necessary. The efficient collection of output photons becomes very critical when the situation turns to a single photon emitter, in which only one photon is emitted at a time. This requirement of Gaussian-like radiation pattern can be fulfilled in micropillar structures [14], [15]. However, Q-factor of such structures is limited to low values due to transverse radiation losses along the pillar cross-section. The Q-factor of such structures can be enhanced by increasing the diameter of the pillar, but doing this yields larger mode volume (V_{eff}). Therefore, the Purcell factor is small. This will lead to low coupling efficiency of the mode into the cavity mode.

To sum up, so as to achieve highly-efficient surface emitting light sources, such as low-threshold nanolasers, and single photon emitters, three requirements, which are high coupling efficiency determined by the Purcell factor, high extraction efficiency, and high collection efficiency determined by the radiation pattern, must be accomplished. So far, it has been reported that there is no single device that can fulfill these three requirements since each one of them holds explicit trade-off.

In this research, a design of photonic crystal slab nanocavity, which can achieve all the requirements, is presented. By just simply optimizing the slab thickness, the dipole mode of the photonic crystal air-bridge H1-defect cavity is shown to have an ability to achieve large Purcell factor, high extraction efficiency, and simple radiation pattern. The design of the H1-defect nanocavity in this research is totally new and original.

1.2 Outline of This Thesis

In this thesis, the design of photonic crystal nanocavity for highly-efficient surface-emitting light sources, is described and organized as follows:

In chapter 2, the theoretical analysis of photonic crystals is reviewed. Starting with mathematical introduction to photonic crystals, Maxwell's equations is fine described. And then, the Bloch-Floquet theorem is described to understand the origin of band structure and band gap of photonic crystals. After that, structure of photonic crystal slab and its band structure are explained. The dependence of its band structure on slab thickness and radius of air holes are also shown. Finally, photonic crystal nanocavity formed by introducing defects to a perfectly periodic system is presented.

In chapter 3, the computational method adopted in this research is described. The computational method is based on the three-dimensional finite-difference time-domain (3D FDTD) method. All characteristics of cavity, e.g., cavity mode frequency, field distribution, Q-factor, and mode volume of defect mode are calculated by using this method.

In chapter 4, firstly, structural parameters and H1-defect structure of the design cavity is described in details. In the design, the dipole mode is exploited as a defect mode. After that, increase of the Q-factor by optimizing the slab thickness is demonstrated. The mechanism of this high Q-factor is discussed in the end of the chapter.

In chapter 5, the efficiency of the dipole mode of the design cavity presented in chapter 4 is investigated. The capability of the dipole mode of the designed H1-defect nanocavity to achieve high efficiency is shown. The result is compared with the highest Q nanocavity reported so far.

In chapter 6, all results are summarized and considered whether the objective of this research is fulfilled. Finally, future prospects are presented.

Chapter 2

Basis for Theoretical Analysis of Photonic Crystal

2.1 Maxwell's Equations and the Bloch-Floquet Theorem

Photonic crystal, which is a periodic arrangement of dielectric media, introduces a periodic potential to photons propagating through it in the same way as a crystal, in which electron experiences a periodic potential due to a periodicity of atoms or molecules, in electronic systems. By cooperating of Maxwell's equations and solid-state physics, the propagation of light in a photonic crystal can be studied. Starting with Maxwell's equations [16]:

$$\vec{\nabla} \times \vec{E} = -\frac{1}{c}\frac{\partial \vec{H}}{\partial t} \tag{2.1}$$

$$\vec{\nabla} \times \vec{H} = \frac{4\pi}{c}\vec{J} + \frac{1}{c}\frac{\partial \varepsilon \vec{E}}{\partial t} \tag{2.2}$$

$$\vec{\nabla} \cdot \varepsilon \vec{E} = 4\pi\rho \tag{2.3}$$

$$\vec{\nabla} \cdot \vec{H} = 0 \tag{2.4}$$

where $\vec{E}$ and $\vec{H}$ are the electric and magnetic fields, which can be expressed by:

$$\vec{E}(\vec{r},t) = \vec{E}(\vec{r})e^{i\omega t} \tag{2.5}$$

$$\vec{H}(\vec{r},t) = \vec{H}(\vec{r})e^{i\omega t} \tag{2.6}$$

$\vec{J}$ is the free current density, ρ is the free charge density, and ε is the dielectric function. In the case that light propagating within a dielectric medium without any light sources, $\vec{J}$ and ρ can be set to zero. In addition, it is acceptable to restrict the dielectric function ε to the case of linear dielectrics. And also, ε is assumed to be independent of frequency and being a real number.

According to these assumptions, by substituting Eq. (2.5) and Eq. (2.6) into Eq. (2.1) and Eq. (2.2) and then combining them together, the result is an equation, which contains only $\vec{H}(\vec{r})$ components:

$$\vec{\nabla}\times\left(\frac{1}{\vec{\varepsilon}(\vec{r})}\vec{\nabla}\times\vec{H}(\vec{r})\right)=\left(\frac{\omega}{c}\right)^2\vec{H}(\vec{r}) \tag{2.7}$$

Then use Eq. (2.2) to regain $\vec{E}(\vec{r})$:

$$\vec{E}(\vec{r})=\left(\frac{-ic}{\omega\vec{\varepsilon}(\vec{r})}\right)\vec{\nabla}\times\vec{H}(\vec{r}) \tag{2.8}$$

It can be observed from Eq. (2.7) that it is a Hermitian eigenvalue problem and can be solved to have a continuous spectrum of eigenfrequencies ω. However, when the case comes to photonic crystal, which is a periodically ordering dielectric media. Dielectric function $\varepsilon(\vec{r})$ then becomes a periodic function of positions. The solution of the Hermitian eigenvalue problem can always be shown in the form of $e^{i\vec{k}\cdot\vec{r}}\cdot$(periodic funtion), where $\vec{k}$ is the wave vector. This is commonly known as Bloch-Floquet theorem [17]. A periodic function is expressed as:

$$\vec{u}_{\vec{k}}(\vec{r})=\vec{u}_{\vec{k}}(\vec{r}+\vec{R}) \tag{2.9}$$

for any lattice vector $\vec{R}$. If the function is periodic in all three dimensions, lattice vector $\vec{R}$ can be formed in, $\vec{R}=l\vec{a}_1+m\vec{a}_2+n\vec{a}_3$, where (l,m,n) are integers and $\vec{a}_1$, $\vec{a}_2$ and $\vec{a}_3$ are primitive lattice vector.

Therefore, the solution of Eq. (2.7) for a periodic dielectric function ε is given by:

$$\vec{H}_{\vec{k}}(\vec{r})=e^{i\vec{k}\cdot\vec{r}}\vec{u}_{\vec{k}}(\vec{r})=e^{i\vec{k}\cdot\vec{r}}\vec{u}_{\vec{k}}(\vec{r}+\vec{R}) \tag{2.10}$$

This Bloch state indicates each electromagnetic mode through its wave vector $\vec{k}$ and periodic function $\vec{u}_{\vec{k}}(\vec{r})$. To solve for $\vec{u}_{\vec{k}}(\vec{r})$, Eq. (2.10) is substituted into Eq. (2.7), another Hermitian eigenvalue problem is then obtained:

$$(\vec{\nabla}+i\vec{k})\times\frac{1}{\varepsilon}(\vec{\nabla}+i\vec{k})\times\vec{u}_{\vec{k}}(\vec{r})=\left(\frac{\omega}{c}\right)^2\vec{u}_{\vec{k}}(\vec{r}) \tag{2.11}$$

Due to the periodicity of $\vec{u}_{\vec{k}}(\vec{r})$, Eq. (2.11) can be considered as the eigenvalue problem over a unit cell of the photonic crystal. Corresponding to quantum mechanics, eigenvalue problem with a finite domain leads to a discrete set of eigenvalues. That is, there is a set of modes, denoted by $\omega_n(\vec{k})$ (for band number n = 1, 2, 3, ...), which are discretely spaced in frequencies and continuously varied as $\vec{k}$ varies. The plot of

these frequency bands as a function of $\vec{k}$ is called the band structure of photonic crystal.

Another important property of the Bloch states is that, in order to solve the eigenvalue problem for a wavevector $\vec{k}$, it is adequate to only solve the eigenvalue problem for $\vec{k}$ in a finite zone called the first Brillouin zone. By considering the Bloch state shown in Eq. (2.10), an eigensolution with wave vector $\vec{k}$ is identical to an eigensolution with wave vector $\vec{k}+\vec{G}$, where $\vec{G}$ is a reciprocal lattice vector and can be evaluated from $\vec{G}\cdot\vec{R} = N2\pi$ (for $N = 1, 2, 3, \ldots$). This means that, in order to solve the eigenvalue problem for $\vec{k}$, $\vec{k}$ will be bounded to only the region in reciprocal space where $\vec{k}$ cannot have any other values of itself by adding any $\vec{G}$. This restricted region is called the first Brillouin zone. Furthermore, if additional symmetries, e.g., rotational symmetry, are applied to photonic crystals, it is unnecessary to solve for every $\vec{k}$ point in the first Brillouin zone. Only the region, in which those symmetries do not have any effects on $\omega_n(\vec{k})$, is required. This region is called the irreducible Brillouin zone.

2.2 The Origin of the Photonic Band Gap

In certain structures of photonic crystal there can be a range of ω, in which no propagating states $\omega_n(\vec{k})$ corresponding to the restricted wave vector $\vec{k}$ are allowed and all incident radiation is reflected. This frequency range is known as the photonic band gap. In order to understand the origin of the gap, two properties of Hermitian eigenvalue problem have to be concerned. Firstly, because the operator of Eq. (2.7) is Hermitian, its eigenvalue must be real and positive and its harmonic modes must be orthogonal:

$$\left\langle \vec{H}_1 \middle| \vec{H}_2 \right\rangle = 0 \tag{2.12}$$

That is, an inner product of any two harmonic modes with different frequencies is zero. Secondly, corresponding to the electromagnetic variational theorem, the lowest frequency mode is the field pattern that minimizes the electromagnetic energy functional:

$$E_f(\vec{H}) = \left(\frac{1}{2(\vec{H},\vec{H})}\right)\int d\vec{r}\,\frac{1}{\varepsilon}\left|\vec{\nabla}\times\vec{H}\right|^2 = \left(\frac{1}{2(\vec{H},\vec{H})}\right)\int d\vec{r}\,\frac{1}{\varepsilon}\left|\frac{\omega\varepsilon}{c}\vec{E}\right|^2 \qquad (2.13)$$

Other higher bands, e.g., the second band, also satisfy Eq. (2.13), but orthogonality of harmonics mode according to Eq. (2.12) must be fulfilled as well. From this expression, in order to minimize E_f, the field of the first band must be concentrated in the regions of high dielectric constant ε to lower its potential energy. This yields to have a lower frequency. Additionally, the curl of field $\vec{\nabla}\times\vec{H}$ should be small, in other words, the field is varying slowly inside the high dielectric constant regions and containing no nodal plane, in order to lower its kinetic energy. When the case comes to the second band, this mode also wants to be concentrated in the high dielectric constant regions and contain no nodal plane inside those regions to obtain the minimum E_f. However, from Eq. (2.12), this mode must be orthogonal to the mode of the first band. As a result, the second band has to be concentrated in the regions of low dielectric constant and restrictedly have nodal plane in those regions to make the integral zero. This results in a difference in frequencies of these two bands and the band gap occurs.

In this thesis, the calculation of band diagram relies on a numerical-analysis method called plane-wave expansion, which solves Maxwell's equations to generate complete band structures and identify band gaps for complex periodic structures.

2.3 Types of photonic crystal

According to the order of dimensions that they periodically alter, photonic crystals can be classified into three categories, which are one-dimensional, two-dimensional, and three-dimensional photonic crystals. These three types of photonic crystal are shown in Fig. 2.1. Straightforward to their names, one-dimensional photonic crystal can only control light at normal incidence to its alternating multilayers, whilst two-dimensional photonic crystal can control light incident from any direction in the plane of periodicity. Complete manipulation of light in three dimensions can be achieved in three-dimensional photonic crystal, which possesses a three-dimensional band gap. Fabricating such an ideal structure, however, has still been a great challenge due to the requirement of highly-advanced structural designs as well as fabrication techniques. Therefore, the system with less restriction

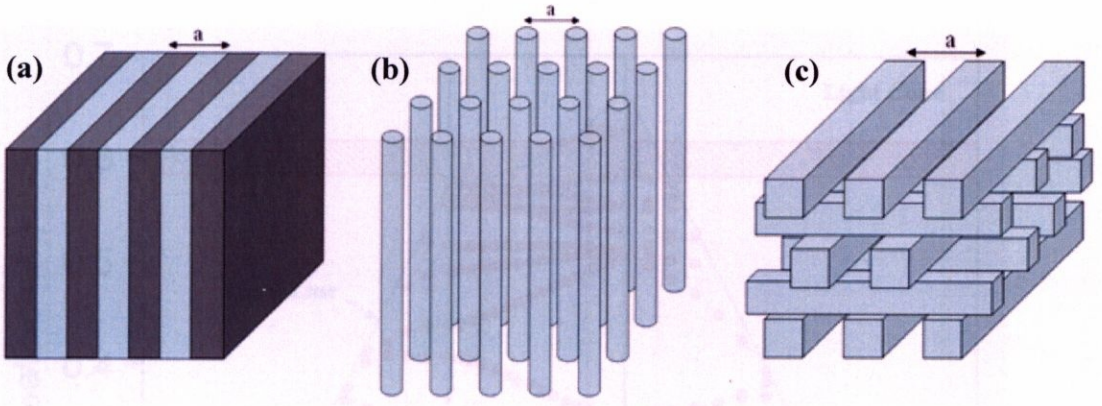

Figure 2.1 Schematic illustrations of photonic crystal (a) one-dimensional (b) two-dimensional (c) three-dimensional.

on designs and fabrication techniques, the photonic crystal slab, is preferable. What is called photonic crystal slab is the dielectric slab with a thickness of the order of the wavelength that has periodicity in two dimensions and is cladded by low-index dielectric in the third direction. Its schematic illustration is shown in Fig. 2.2. Hence the light manipulation in photonic crystal slab is a combination of Bragg reflection from the two-dimensional photonic crystal and total internal reflection from the low-index cladding results in a three-dimensional control of optical modes.

2.4 Band Structures of Photonic Crystal Slab

Band structure for photonic crystal slab is slightly different from that of two-dimensional photonic crystal because band structure computed for a two-dimensional photonic crystal corresponds only to the modes, in which the

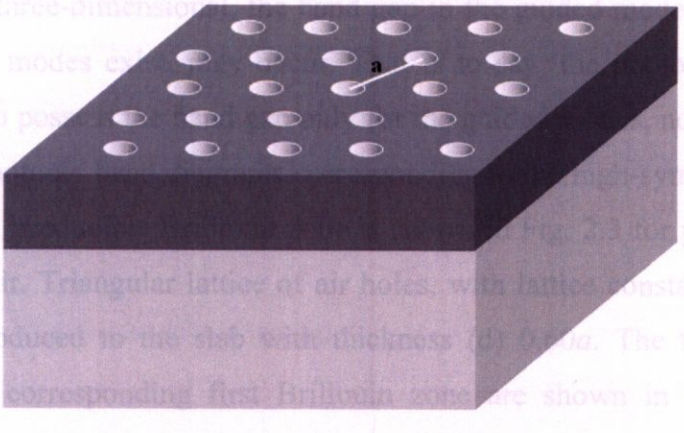

Figure 2.2 Schematic illustration of photonic crystal slab structure. Dark grey layer is a slab waveguide cladded by claddings. Air holes are also depicted in the figure.

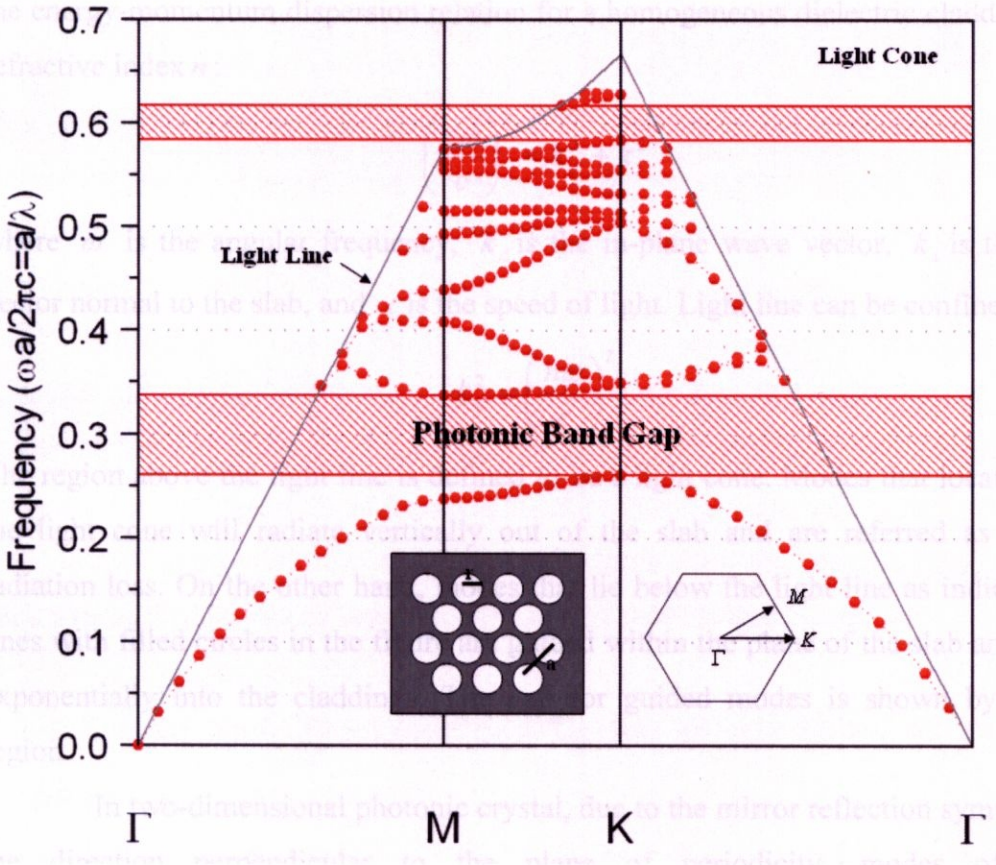

Figure 2.3 Band diagram for the air-bridge slab structure with $r = 0.30a$ and $d = 0.60a$. The insets show triangular lattice of air holes in dielectric with refractive index of 3.4 and its first Brillouin zone.

consideration of wave vector in the direction perpendicular to the plane of periodicity is not included. Furthermore, finite stretch of photonic crystal slab structure in the third direction destroys the band gap of the two-dimensional structure. By considering the system to be three-dimensional, the band gap in the guided modes of the slab, in which no guided modes exist, may occur. That is to say, the photonic crystal slab structure is able to possess the band gap only for the guided modes, not for all modes. An example of photonic band diagrams corresponding to the high-symmetry points at the corners of the irreducible Brillouin zone is shown in Fig. 2.3 for photonic crystal slab cladded by air. Triangular lattice of air holes, with lattice constant a and radius (r) $0.30a$, is introduced to the slab with thickness (d) $0.60a$. The top-view of the structure and its corresponding first Brillouin zone are shown in the insets. The refractive index of the high index material is 3.4. Band structure of the photonic crystal slab is composed of two regions, guided mode region and light cone. They are separated by light line depicted as the dark line in the figure. Concretely, examining

the energy-momentum dispersion relation for a homogeneous dielectric cladding with refractive index n:

$$\left(\frac{n\omega}{c}\right)^2 = k_{\angle}^2 + k_{\perp}^2 \tag{2.14}$$

where ω is the angular frequency, $k_{\angle}$ is the in-plane wave vector, $k_{\perp}$ is the wave vector normal to the slab, and c is the speed of light. Light line can be confined as:

$$k_{\angle}^2 = \left(\frac{n\omega}{c}\right)^2 \tag{2.15}$$

The region above the light line is defined to be a light cone. Modes that locate inside the light cone will radiate vertically out of the slab and are referred as vertical radiation loss. On the other hand, modes that lie below the light line as indicated by lines with filled circles in the figure are guided within the plane of the slab and decay exponentially into the claddings. The gap for guided modes is shown by shaded region.

In two-dimensional photonic crystal, due to the mirror reflection symmetry in the direction perpendicular to the plane of periodicity, modes of every two-dimensional photonic crystal can be classified into two non-interacting classes of polarizations: TE polarized modes (electric field in plane of periodicity) and TM polarized modes (magnetic field in plane of periodicity). As in two-dimensional system, guided modes in photonic crystal slab can be also decomposed into two distinct classes. These are not purely TE and TM polarized as in the two-dimensional photonic crystal due to the finite extent of slab in the direction normal to the plane of slab. However, they are classified by whether they transform to be even or odd with respect to a horizontal mirror plane bisecting the slab. These even and odd states have the strong similarities with TE and TM modes, respectively, in two-dimensional photonic crystal. In addition, within the slab they are TE- and TM-like, and closely resemble the TE and TM modes in two-dimensional system.

2.5 Air-Bridge Photonic Crystal Slab

A significant issue of photonic crystal slab is its cladding. Photonic crystal slab uses the mechanism of waveguide originated from the refractive index difference of material of slab and cladding to confine light in the third dimension. However, in the perforating air holes, which are etched through the slab and cladding layers, there

is no refractive index in the vertical direction. These air holes can cause the out-of-plane scattering loss from the slab to the cladding. In order to minimize this loss, high-index contrast system is preferable, especially the structure of dielectric slab suspended in air, which is called air-bridge structure. With this high contrast, Bloch modes that lie well below the light line can be created. This leads to no coupling of these modes to the radiation continuum located within light cone.

According to the active regions of most conventional devices, such as quantum wells and quantum dots, have the electronic states that predominantly couple to the TE modes, photonic crystal slabs that support TE-like modes are preferable. More concretely, air-bridge dielectric slabs with two-dimensional triangular lattice of air holes are appropriate for this situation because they can support large photonic band gap in TE-like modes separating the lowest two TE-like bands.

2.6 Effect of Slab Thickness and Radius of Air Holes on Photonic Band Gap

As already mentioned, a two-dimensional photonic crystal slab has a band gap in its guided modes. Among many photonic band gaps that can occur, the lowest-order photonic band gap that emerges between the lowest-order mode and the second-order mode is the most interesting due to lower density of radiation states in low frequency region. However, this band gap can occur only when some of parameters of the slab are suitable. More concretely, if radius of the air holes (r) is large enough as well as appropriate slab thickness (d) is fulfilled, the gap may appear [18], [19]. The radius of air holes has an important effect on the propagation in the slab, as it determines the width of the gap. Increase of radius of air holes over the appropriate range (for example, not over than $0.40a$) results in increase of the gap size [18]. Figure 2.4 shows the plots between the gap-mid gap ratio, which designates the band gap size, for and the slab thickness for even modes in the air-bridge structure with r equal to $0.30a$, $0.35a$, and $0.40a$ indicated by boxed dots, circular dots, and triangular dots, respectively. The structure with $r = 0.40a$ yields the largest gap size, while structure with $r = 0.30a$ has the narrowest gap over the range of slab thickness less than $0.60a$. When the slab thickness is over $0.60a$, the tendency of gap size becomes complex. This is because when the slab is thick, the gap is determined by the frequency range between the lowest-order band edge and the second-order waveguide

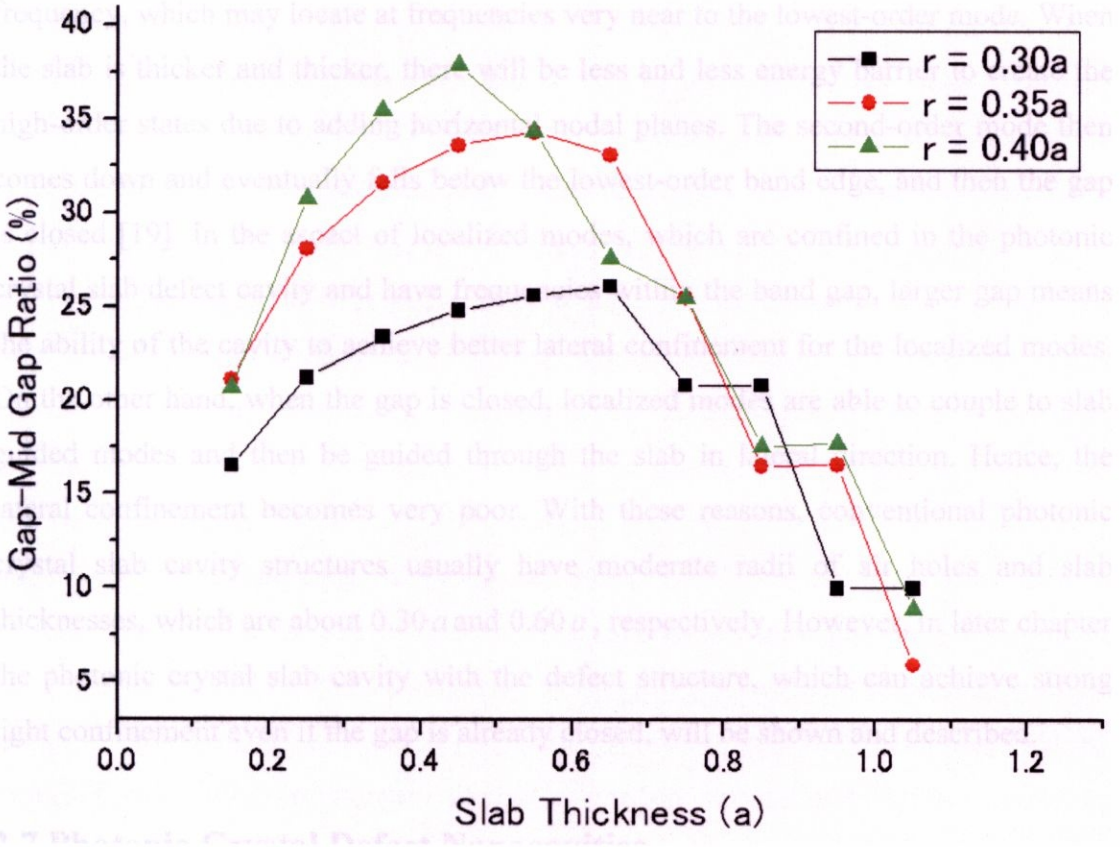

Figure 2.4 Dependence of Gap-mid gap ratio on slab thickness for air-bridge slab structure with $r = 0.30a$ (square), $r = 0.35a$ (circle), and $r = 0.40a$ (triangle).

mode cutoff, instead of the frequency range between the lowest-order band edge and the band edge at K point of the first Brillouin zone in the case of the slab thinner than $0.60a$. In the calculation of band structure, accurate values of the cutoff frequency are difficult to calculate. Hence, the exact results are a little inconsistent. Generally, larger gap is preferable in most of applications. However, increase of radius of air holes is also followed by an increase of coupling losses in the in-plane direction [20]. This increase of losses is due to decrease in effective index of the mode compared to that of the imperforated guided mode.

The other way to engineer the band gap is to change the thickness of the slab. The existence of the gap and the gap size strongly depends on the slab thickness as shown in Fig. 2.4. It is obvious that there is an optimal slab thickness, which can yield the largest gap between the first two bands. When the slab is too thin, air holes are just like a weak perturbation on the bare slab. Guided modes will still exist, but they cannot be strongly confined within the slab. As a result, the gap is very small. On the other hand, if the slab is too thick, the second-order modes will be created at low

frequency, which may locate at frequencies very near to the lowest-order mode. When the slab is thicker and thicker, there will be less and less energy barrier to create the high-order states due to adding horizontal nodal planes. The second-order mode then comes down and eventually falls below the lowest-order band edge, and then the gap is closed [19]. In the aspect of localized modes, which are confined in the photonic crystal slab defect cavity and have frequencies within the band gap, larger gap means the ability of the cavity to achieve better lateral confinement for the localized modes. On the other hand, when the gap is closed, localized modes are able to couple to slab guided modes and then be guided through the slab in lateral direction. Hence, the lateral confinement becomes very poor. With these reasons, conventional photonic crystal slab cavity structures usually have moderate radii of air holes and slab thicknesses, which are about $0.30\,a$ and $0.60\,a$, respectively. However, in later chapter, the photonic crystal slab cavity with the defect structure, which can achieve strong light confinement even if the gap is already closed, will be shown and described.

2.7 Photonic Crystal Defect Nanocavities

Analogy to the electronic systems, introducing a defect to the photonic crystal lattice may permit a single or a set of localized modes, which have frequencies in the photonic band gap. Consequently, the defect-induced mode cannot penetrate the unperturbed crystal and is then confined in the defect region. With this concept, photonic crystal cavity is able to be created. In the case of photonic crystal slab with air holes, the simplest defect cavity may be formed by removing a single hole in the photonic crystal. The resonant mode with frequency locating inside the gap is highly localized to the defect region, and light can only escape by either tunneling through the two-dimensional photonic crystal or by impinging on the cladding-slab interface to leak out from the cavity. However, a band gap in this kind of structure prohibits only guided modes to exist, not a true band gap. To be specific, at the frequencies of defect-induced localized-modes, there are still radiation modes. These radiation modes correspond to the mode locating above the light line as previously mentioned. As a result, the resonant cavity mode will eventually decay into the cladding. The quality factor (Q-factor) is usually exploited to designate how well the cavity can confine light before it decays out of the cavity.

2.8 Summary

In this chapter, the principle of photonic crystal has been reviewed theoretically. By cooperating of Maxwell's equations and solid-state physics, the propagation of light in a photonic crystal can be studied. Due to a periodic dielectric function of photonic crystal, the Bloch-Floquet theorem can then be applied to solve the Hermitian eigenvalue problem over a unit cell of the photonic crystal. The solution results in a discrete set of modes, which originates a band structure of the photonic crystal. In addition, by considering the electromagnetic variation theorem, the origin of the photonic band gap, in which no propagating modes can be existed, has been revealed. After that, the photonic crystal slab structure, which is a combination of a conventional waveguide and a two-dimensional photonic crystal, has been described in details. Its band structure shows that band gaps of guided modes can be obtained in this kind of structure. The light cone, which is a cause of vertical radiation loss in the photonic crystal slab structure, has also been clarified by examining the energy-momentum dispersion relation. Among many types of cladding materials of photonic crystal slab, air-bridge structure is expected to be able to suppress the out-of-plane scattering loss from the slab to the cladding. The dependence of its photonic band gap size on slab thickness and radius of air holes has been shown. Finally, photonic crystal nanocavities formed by introducing defects to a perfectly periodic system have been presented.

Chapter 3

Three-Dimensional Finite-Difference Time-Domain Method

3.1 Three-Dimensional Finite-Difference Time-Domain Method

The calculation method exploited in modeling optical characteristics of structures described above is the three-dimensional Finite-Difference Time-Domain (3D FDTD) method [21], which is based on a discretization of the Maxwell's time dependent curl equations, e.g., Eq. (2.1) and (2.2). A Cartesian spatial grid is defined with increments Δx, Δy, and Δz, and Δt is a time increment. Any field u of space (i, j, k) and time t is evaluated at a discrete point in space and time as:

$$u^n_{i,j,k} = u(i\Delta x, j\Delta y, k\Delta z, n\Delta t) \tag{3.1}$$

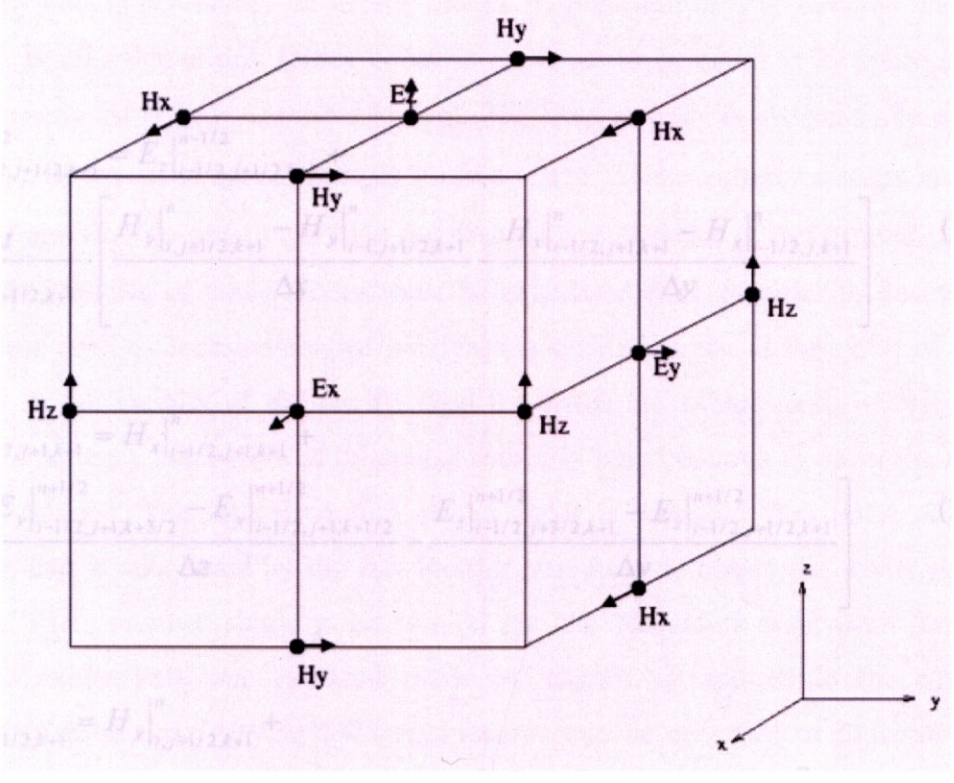

Figure 3.1 Positions of field components using Yee's cell.

where n is an integer. A schematic, corresponding to the Yee's algorithm, representing positions in space of the electric and magnetic field vector components is shown in Fig. 3.1. In addition, all field components are advanced in time, using a leapfrog algorithm. As a result, the electric and magnetic fields are located at the positions that are differed by half a step in both space and time. Six finite-difference equations for each of the electromagnetic fields are then solved and shown as [22]:

$$E_x\Big|_{i,j+1/2,k+1/2}^{n+1/2} = E_x\Big|_{i,j+1/2,k+1/2}^{n-1/2} + \frac{\Delta t}{\varepsilon_{i,j+1/2,k+1/2}} \cdot \left[\frac{H_z\Big|_{i,j+1,k+1/2}^{n} - H_z\Big|_{i,j,k+1/2}^{n}}{\Delta y} - \frac{H_y\Big|_{i,j+1/2,k+1}^{n} - H_y\Big|_{i,j+1/2,k}^{n}}{\Delta z} \right] \tag{3.2}$$

$$E_y\Big|_{i-1/2,j+1,k+1/2}^{n+1/2} = E_y\Big|_{i-1/2,j+1,k+1/2}^{n-1/2} + \frac{\Delta t}{\varepsilon_{i-1/2,j+1,k+1/2}} \cdot \left[\frac{H_x\Big|_{i-1/2,j+1,k+1}^{n} - H_x\Big|_{i-1/2,j+1,k}^{n}}{\Delta z} - \frac{H_z\Big|_{i,j+1,k+1/2}^{n} - H_z\Big|_{i-1,j+1,k+1/2}^{n}}{\Delta x} \right] \tag{3.3}$$

$$E_z\Big|_{i-1/2,j+1/2,k+1}^{n+1/2} = E_z\Big|_{i-1/2,j+1/2,k+1}^{n-1/2} + \frac{\Delta t}{\varepsilon_{i-1/2,j+1/2,k+1}} \cdot \left[\frac{H_y\Big|_{i,j+1/2,k+1}^{n} - H_y\Big|_{i-1,j+1/2,k+1}^{n}}{\Delta x} - \frac{H_x\Big|_{i-1/2,j+1,k+1}^{n} - H_x\Big|_{i-1/2,j,k+1}^{n}}{\Delta y} \right] \tag{3.4}$$

$$H_x\Big|_{i-1/2,j+1,k+1}^{n+1} = H_x\Big|_{i-1/2,j+1,k+1}^{n} + \frac{\Delta t}{\mu_0} \cdot \left[\frac{E_y\Big|_{i-1/2,j+1,k+3/2}^{n+1/2} - E_y\Big|_{i-1/2,j+1,k+1/2}^{n+1/2}}{\Delta z} - \frac{E_z\Big|_{i-1/2,j+3/2,k+1}^{n+1/2} - E_z\Big|_{i-1/2,j+1/2,k+1}^{n+1/2}}{\Delta y} \right] \tag{3.5}$$

$$H_y\Big|_{i,j+1/2,k+1}^{n+1} = H_y\Big|_{i,j+1/2,k+1}^{n} + \frac{\Delta t}{\mu_0} \cdot \left[\frac{E_z\Big|_{i+1/2,j+1/2,k+1}^{n+1/2} - E_z\Big|_{i-1/2,j+1/2,k+1}^{n+1/2}}{\Delta x} - \frac{E_x\Big|_{i,j+1/2,k+3/2}^{n+1/2} - E_x\Big|_{i,j+1/2,k+1/2}^{n+1/2}}{\Delta z} \right] \tag{3.6}$$

$$H_z\Big|_{i,j+1,k+1/2}^{n+1} = H_z\Big|_{i,j+1,k+1/2}^{n} +$$
$$\frac{\Delta t}{\mu_0}\cdot\left[\frac{E_x\Big|_{i,j+3/2,k+1/2}^{n+1/2} - E_x\Big|_{i,j+1/2,k+1/2}^{n+1/2}}{\Delta y} - \frac{E_y\Big|_{i+1/2,j+1,k+1/2}^{n+1/2} - E_y\Big|_{i-1/2,j+1,k+1/2}^{n+1/2}}{\Delta x}\right] \tag{3.7}$$

In order to obtain efficient and accurate solution of electromagnetic waves as if the computational domain is unbounded and stretches to the infinity, the perfectly matched layer (PML) must be introduced at all outer boundaries as a nonreflecting absorber [23]. PML creates a nonphysical absorbing material, which can absorb the electromagnetic waves without reflection for any frequency, polarization, and angle of incidence at the interfaces between the PMLs and the FDTD computational domains.

3.2 Calculation of Cavity Characteristics by using the 3D FDTD Method

By using the 3D FDTD calculation, resonant frequencies, field distributions, and quality factor (Q-factor) of defect modes in photonic crystal cavities can be evaluated. In all calculations, lattice constant (a) is set to be equal to 20 space steps ($20\Delta x$), where $\Delta x = \Delta y = \Delta z$ (cubic lattice). The time step Δt is chosen to be equal to $\Delta x/(2c)$, where c is speed of light in free space. These values of steps ensure numerical stability. To obtain the field distribution and Q-factor of defect modes, the resonant frequencies of those modes must be calculated first. In order to do this, a pulse source with a Gaussian-shaped bandpass is excited in the at the point of low symmetry in the vicinity of the cavity, then the fields are subsequently evolved in time. The frequency bandwidth of this pulse source is broad enough to cover the total modes of interest. The time evolution of the fields is recorded at a point of low symmetry, and is calculated by the fast Fourier transform to obtain the cavity mode spectrum. Then, another single pulse, which has the frequency bandwidth narrow enough to excite only one resonant mode of interest, is applied to the cavity. Snap-shot of each time-varying field components can be recorded to illustrate the point-in-time view of field distributions of the resonant mode. The Q-factor is obtained by measuring the exponential decay of electromagnetic energy after turning off the oscillation of the source [24]:

$$U(t) = U(0)\exp(-t/\tau_{ph}) = U(0)\exp[-(\omega_0 t)/Q] \tag{3.8}$$

where $U(t)$ is the electromagnetic energy in the mode at time t, and ω_0 is the frequency of the cavity mode. The total Q-factor is evaluated by measuring the slope of the logarithm plot of this energy-time relation. In order to efficiently determine what factors are limiting the Q-factor of the defect modes, another calculation method is adopted to separate out the radiation losses into different directions, vertical and in-plane directions, which are due to leaky modes and lack of number of photonic crystal layers that surround the defect region, respectively. In other words, the total radiating power P can be divided in to vertical radiation $P_\perp$ and in-plane radiation $P_\angle$. The total radiating power $P = P_\perp + P_\angle$ is related to the electromagnetic energy $U(t)$ by [24]:

$$P = -\frac{dU}{dt} = \frac{\omega_0 U}{Q} \tag{3.9}$$

where ω_0 is the angular frequency of the cavity mode. As a result, the total Q-factor can be separated into vertical and in-plane components, denoted as $Q_\perp$ and $Q_\angle$, respectively, and satisfy the following relation:

$$\frac{1}{Q} = \frac{1}{Q_\perp} + \frac{1}{Q_\angle} \tag{3.10}$$

Combine the relations in Eq. (3.9) and Eq. (3.10), the Q-factor in each direction are then given by [25]:

$$Q_{\perp,\angle} = \frac{\omega_0 U}{P_{\perp,\angle}} \tag{3.11}$$

In practical calculation, these effective Q values are calculated by spatial separation of the power radiated by the mode that is absorbed in the outer boundary [25]. The in-plane radiation $P_\angle$ is defined as the Poynting vector that is absorbed into the sidewalls that extend from approximately a half-wavelength above the waveguide to a half-wavelength below the waveguide. The vertical radiation $P_\perp$ is defined as the Poynting vector that is absorbed into the rest of the boundary.

The Purcell factor [1], which indicates strength of interaction between electromagnetic field and emitters inside a cavity, and the mode volume are calculated using the following definition:

$$F_p = \frac{3Q}{4\pi^2 V_{eff}} \left(\frac{\lambda}{n}\right)^3 \tag{3.12}$$

$$V_{eff} = \frac{\iiint \varepsilon(\vec{r}) \left|\vec{E}(\vec{r})\right|^2 d^3\vec{r}}{\max[\varepsilon(\vec{r}) \left|\vec{E}(\vec{r})\right|^2]} \tag{3.13}$$

where n is the refractive index of a cavity, $\varepsilon(\vec{r})$ is the dielectric constant at position $\vec{r}$, and $\vec{E}(\vec{r})$ is the total electric field at position $\vec{r}$.

3.3 Summary

In this chapter, details of the calculation method based on the three-dimensional finite-difference time-domain (3D FDTD) method have been described. The computational model was bounded by the perfectly matched layer in order to obtain efficient and accurate solution of electromagnetic waves. Then, the application of the 3D FDTD method to investigate the characteristics of cavity, such as, resonant frequency, field distribution, Q-factor, Purcell factor, and mode volume, of defect mode has been shown. The computational methods described in this chapter will be applied to the calculation of all structures in the following chapters.